Electronic Supplementary Material (ESI) for Sustainable Energy & Fuels.

Supplementary Information

Assessing the True Power of Bifacial Perovskite Solar Cells under Concurrent Bifacial Illumination

Zhaoning Song, Cong Chen, Chongwen Li, Suman Rijal, Lei Chen, You Li, and Yanfa Yan**

Department of Physics and Astronomy and Wright Center for Photovoltaics Innovation and Commercialization, The University of Toledo, Toledo, Ohio 43606, United States

AUTHOR INFORMATION

Corresponding Author

*zhaoning.song@utoledo.edu and yanfa.yan@utoledo.edu

Experimental Section

Perovskite Precursor Preparation: The perovskite precursor solution was prepared following our previous work.[1] In brief, to achieve a desired composition of $FA_{0.8}Cs_{0.2}Pb(I_{0.9}Br_{0.1})_3$, 138 mg formamidinium iodide (FAI, Greatcell Solar), 52 mg cesium iodide (CsI, Alfa Aesar), 392 mg lead iodide (PbI_2, TCI), 55 mg lead bromide ($PbBr_2$, TCI), and 5.2 mg lead thiocyanate ($Pb(SCN)_2$, Sigma-Aldrich) were dissolved in a mixed solvent of 600 mL N,N-dimethylformamide (DMF, Sigma-Aldrich) and 200 mL dimethyl sulfoxide (DMSO, Sigma-Aldrich) and stirred for 5 h before use.

Solar Cell Fabrication: 1" by 1" ITO substrates (15 Ω/sq) were cleaned sequentially in an ultrasonic batch using diluted Micro-90 detergent, deionized water, acetone, and isopropanol for 15 min each. The cleaned ITO substrates were dried by a nitrogen flow and further treated in an ultraviolet-ozone cleaner (Novascan) for 20 min and then transferred to a nitrogen-filled glovebox for device fabrication. First, A 4 mg/mL poly(triarylamine) (PTAA, Sigma-Aldrich) in chlorobenzene (Sigma-Aldrich) solution was spin-coated on ITO substrates at 6,000 rpm for 30 s and annealed at 100 ℃ for 10 min. After the substrates cooled down, a 0.5 mg/ml PFN-Br (1-Material) in methanol (Sigma-Aldrich) solution was spin-coated at 4,000 rpm for 30 s. To deposit perovskite films, 80 μL perovskite precursor solution was spin-coated at 500 rpm for 2 s and at 4000 rpm for 60 s. At the 30 s of the second step, 750 μL diethyl ether (Sigma-Aldrich) as anti-solvent was dripped onto the spinning substrate. The as-prepared films were then annealed at 65 ℃ for 2 min and 100 ℃ for 10 min. After cooling down, the films were coated with a 2 mg/ml 2-phenylethylammonium iodide (PEAI, Greatcell Solar) in isopropanol (Sigma-Aldrich) solution by spin-coating at 3,000 rpm for 30 s. After that, a 20 nm fullerene (C_{60}, nano-c) was evaporated in a vacuum chamber with a base pressure of less than 1×10^{-6} Torr. A 20 nm SnO_2 layer was then deposited by thermal atomic layer deposition (ALD, Ensure Scientific) following a reported method.[2] A 150 nm ITO layer (sheet resistance = 28 Ω/sq) was sputtered through a shadow mask using a 3″ target (Lesker) at a power of 90 W under 2 mTorr Ar pressure, followed by a 250 nm Ag metal grid deposited by thermal evaporation through a matched shadow mask. For the antireflection coatings, 120 nm magnesium fluoride (MgF_2, Sigma Aldrich) films were sequentially deposited on both the glass side and the sputtered ITO side by e-beam evaporation. The active area of devices is 0.25 cm^2, as defined by the area of the sputtered ITO patterns. The Ag grids are aligned on the fringes of the sputtered ITO patterns.

Device Characterization: Current density-voltage (J-V) curves of solar cells were measured by a Keithley 2400 source meter. For conventional J-V measurement under monofacial illumination, a solar simulator (PV Measurements Inc.) was used to generate AM1.5G (100 mW/cm^2) illumination. For concurrent bifacial J-V measurements, a LED solar simulator (Newport) was used to simulate the direct sunlight with an AM1.5G spectrum, while a fiber optic illuminator with a mirror was used to simulate albedo light with various light intensity (0 to 50 mW/cm^2). Both front and read illumination sources are adjusted to the normal incident direction. Light intensity for both front and back illumination was calibrated using a NIST certified standard Si cell. For J-V measurements, two apertures of 0.22 cm^2 (4.7 mm x 4.7 mm) were applied on both sides of a bifacial cell to define the illuminated area. External quantum efficiency (EQE) spectra

were obtained with a QE system (PV Measurements Inc.). Device stability tests were performed using a commercial maximum power point tracking system (CandleLight).

EQE Simulation: EQE simulations were generated and compared to experimental results using e-ARC software (version 2.02) made by The National Institute of Advanced Industrial Science and Technology (AIST), Japan. The optical properties used for the simulation were obtained from our previous work.

Detailed balance efficiency calculation: Detailed balance efficiency calculations for bifacial solar cells were performed based on the work of Shockley and Queisser.[3] In brief, for an ideal solar cell, the total rate of recombination at the short circuit condition is only determined by the blackbody radiation from both sides of the cell with energy above its bandgap. The dark saturated current density (J_0) can be approximated to:

$$J_0 = 2q\int_{E_g}^{\infty} \frac{1}{\exp(h\nu/kT) - 1}\frac{2\pi\nu^2}{c^2}d\nu ,$$

where q is the unit charge, E_g is the bandgap of the solar cell, h is the Planck constant, k is the Boltzmann constant, T is the temperature of the cell, ν is the photon frequency, and c is the speed of light.

The short-circuit photocurrent density (J_{SC}) of an ideal bifacial solar cell can be calculated by

$$J_{SC} = \int_{\lambda_i}^{1240/E_g} [I_0(\lambda) + I_{albedo}(\lambda) \times B]d\lambda ,$$

where $I_0(\lambda)$ is the AM1.5G solar spectrum, $I_{albedo}(\lambda)$ is the albedo light spectrum, B is bifaciality of the bifacial solar cell, λ_i is the shortest wavelength for the illumination spectra, and E_g has a unit of eV. For the calculation, an experimentally determined bifaciality of 0.96 was used. For the calculations with different albedo materials (Figure S5 and 2), reflectance spectra were obtained from the ASTER spectral library.[4] For uniform albedo calculations (Figure S8), a uniform albedo of 0.1 to 0.5 was used.

The J-V curve of an ideal solar cell can be calculated by the Shockley diode equation:

$$J = J_0\left[\exp\left(\frac{V}{kT}\right) - 1\right] - J_{SC} .$$

Solar cell parameters can thus be extracted from the J-V curves for different absorber bandgaps and albedo light conditions. Particularly, the equivalent bifacial efficiency is determined by:

$$\eta(E_g, albedo) = \frac{V_{mpp}(E_g,\ albedo) \times J_{mpp}(E_g, albedo)}{100\ mW/cm^2} \times 100\% ,$$

where J_{mpp} and V_{mpp} are current density and voltage values at the maximum power point. The equations above were numerically solved in a bandgap range of 0.5 to 2.5 eV with a step size of 0.05 eV using a customized Igor Pro program.

It is worth noting that V_{OC} and FF of a non-ideal bifacial solar cell can be influenced by albedo light intensity. A higher photocurrent induced by increasing albedo light intensity increases the thermal energy loss at the series resistance ($P_{loss} = JR_s^2$) and therefore decreases the FF of a solar cell. The change of FF can be estimated by Green's classical theoretical FF expression:[5]

$$FF_s = FF_0 \cdot (1 - \frac{R_S \cdot J_{SC}}{nKT/q \cdot Ln(J_{SC}/J_0)})$$

where FF_0 and FF_S are fill factors of an ideal and non-ideal solar cell, R_S is series resistance, n is ideality factor of a solar cell, k is Boltzmann constant, T is the temperature, q is the unit charge. This expression shows that increasing J_{SC} leads to decreasing FF.

On the other hand, Increasing J_{SC} increases V_{OC}, as determined by the equation below:

$$V_{OC} = \frac{nkT}{q} Ln(\frac{J_{SC}}{J_0} + 1)$$

Supplementary Data

Table S1. Bifacial perovskite solar cell applications reported in the literature.

Device Structure	E_g (eV)	Area (cm^2)	PCE (%)	V_{OC} (V)	J_{SC} ($mA \cdot cm^{-2}$)	FF (%)	Bifaciality	Note
Glass/ITO/PEDOT/sorbitol/Spiro-OMeTAD/ $MAPbI_3/SnO_2$/ITO/glass	1.58	0.15	15.8	1.04	20.6	72.8	0.93	Ref. [6]
Glass/ITO/SnO_2/FAMACs-perovskite/ Spiro-OMeTAD/MoO_x/Ag/WO_x	1.6	0.1	15.4	1.03	22.8	66	0.63	Ref. [7]
Glass/FTO/TiO_2/ $Cs_{0.05}(MA_{0.17}FA_{0.83})_{0.95}$ $Pb(I_{0.83}Br_{0.17})_3$ /CuSCN/ITO	1.62	0.16	14.2	0.98	20.2	72.1	0.94	Ref. [8]
Glass/ITO/NiOx/ $FA_{0.3}MA_{0.7}PbI_{3-x}Cl_x$ /PCBM/BCP/ultrathin Ag/ TeO_2	1.57	0.07	20.3	1.12	22.5	80.3	0.83	Ref. [9]
		1.0	12.4	1.14	16.4	66.5	0.85	
Glass/ITO/SnO_2/$MAPbI_3$/Spiro-OMeTAD/ITO	1.58	~0.1	16.7	1.01	23.4	70.7	0.57	Ref. [10]
Glass/FTO/TiO2/PCBM/$FA_{0.75}Cs_{0.25}Pb$ $(I_{0.8}Br_{0.2})_3$/Spiro-OMeTAD/ITO/MgF_2/Au grid	~1.7	0.25	14.7	1.17	17.3	73	0.93	Ref. [11]
Glass/ITO/PEDOT:PSS/$Cs_{0.05}FA_{0.3}$ $MA_{0.7}PbI_{2.51}Br_{0.54}$/PCBM/BCP/Ag /$V_2O_5$	1.57	0.07	14.0	1.00	17.9	77.7	0.64	Ref. [12]
Glass/ITO/PEDOT:PSS/$MAPbI_3$/PCBM/BCP/Ag/MoO_3	1.58	0.1	13.5	1.05	17.7	72.5	0.71	Ref. [13]
Glass/FTO/TiO_2/$CsPbBr_3$/Carbon /$CsPbBr_3$/TiO_2/FTO/Glass	2.3	0.02	7.55	1.39	7.1	77	0.99	Ref. [14]
Glass/In_2O_3:H/PTAA/$MAPbI_3$/PCBM/ ZnO/ZnO:Al/Ni–Al grid	1.58	0.286	16.1	1.12	19.1	75.4	0.99	Ref. [15]
MgF_2/glass/ITO/PTAA/$FA_{0.8}Cs_{0.2}Pb(I_{0.9}Br_{0.1})_3$/$C_{60}$/$SnO_2$/ITO/Ag grid/$MgF_2$	1.6	0.22	18.4	1.12	20.4	80.2	0.96	This work, single side illumination
		0.22	26.1	1.17	29.6	75.8	NA	Bifacial illumination with an albedo of 0.5

*Note: This table only surveys bifacial perovskite solar cells with reported J-V and EQE curves from both the front and back illumination.

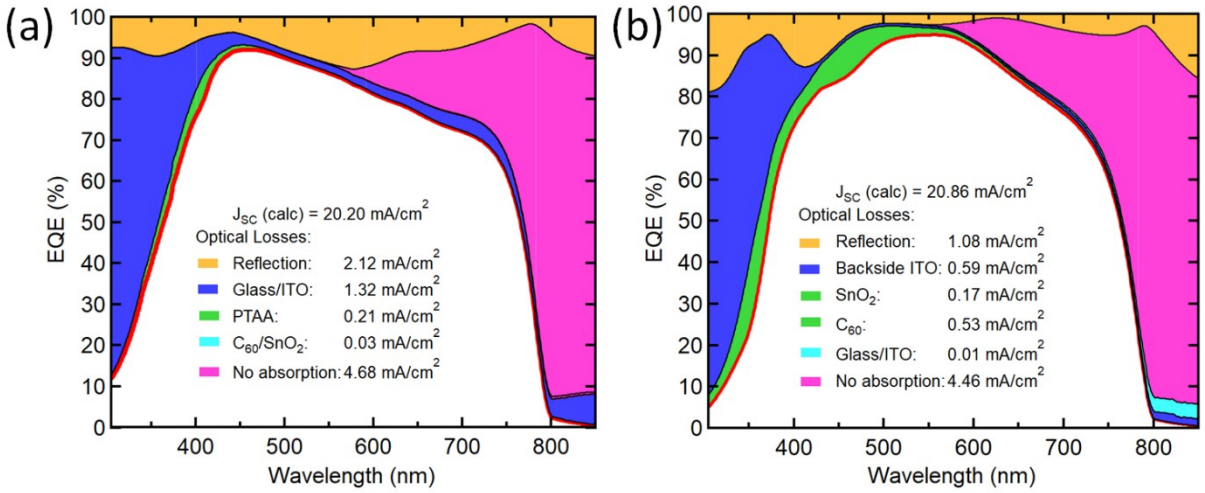

Figure S1. EQE simulation and loss analysis of bifacial PSCs under (a) glass-side and (b) film-side illumination. The simulation results show that a bifaciality of 1 is achievable in this device configuration with proper optimization of each component layer thickness.

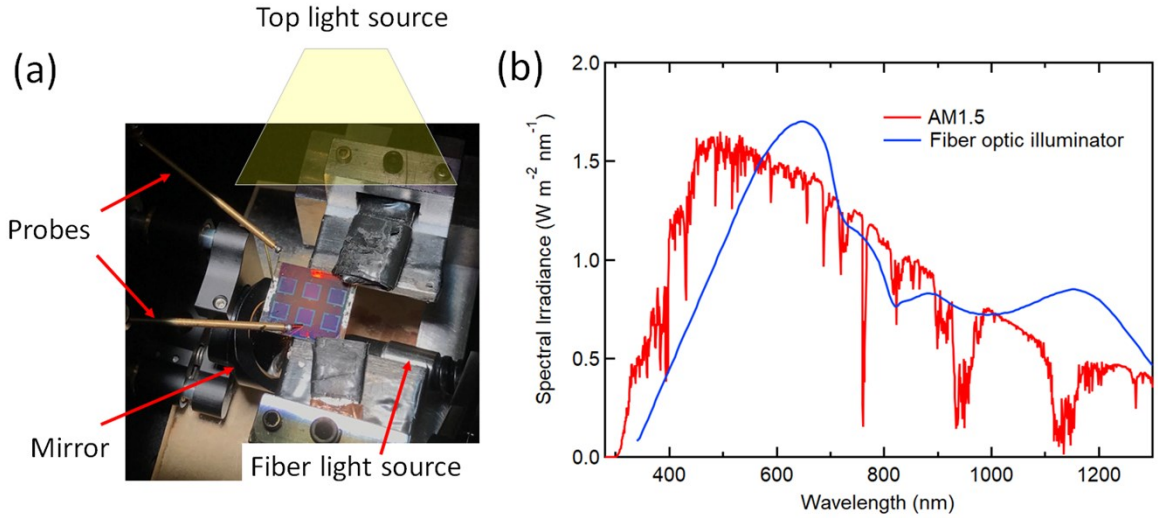

Figure S2. (a) Example of J-V measurement of a bifacial PSC under concurrent bifacial illumination. The aperture is not included in this photo. (b) Irradiance spectrum of fiber optic illuminator used for the simulated albedo light.

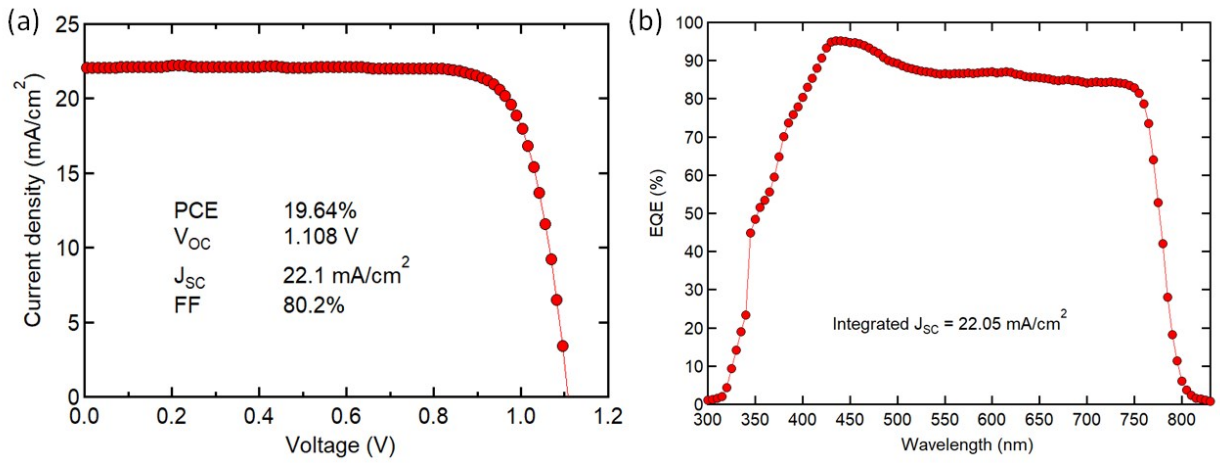

Figure S3. J-V and EQE curves of a typical PSC with an opaque back electrode.

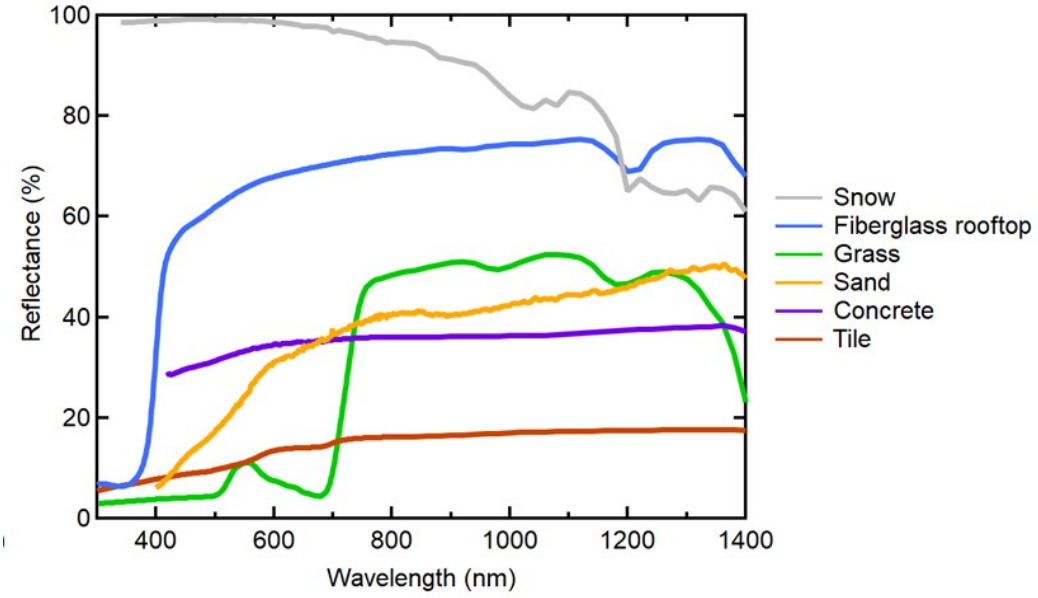

Figure S4. Albedo spectra of different ground materials, including snow, fiberglass rooftop, grass, yellow sand, concrete, and tile. The reflectance data is adapted from NASA's ECOSTRESS Spectral Library.

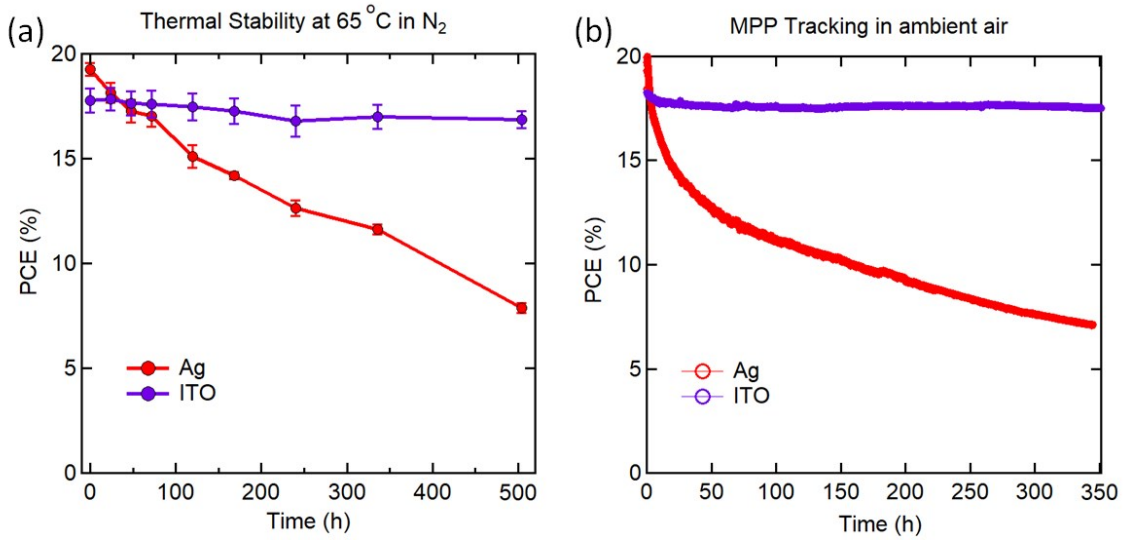

Figure S5. Stability test of PSCs. (a) Thermal stability test of PSCs with Ag and ITO as the back electrode at 65 ˚C in nitrogen. The results are an average of 3 cells for each group. (b) Maximum power point tracking under simulated AM 1.5 spectrum in ambient air (~50 ˚C, RH =30-50%).

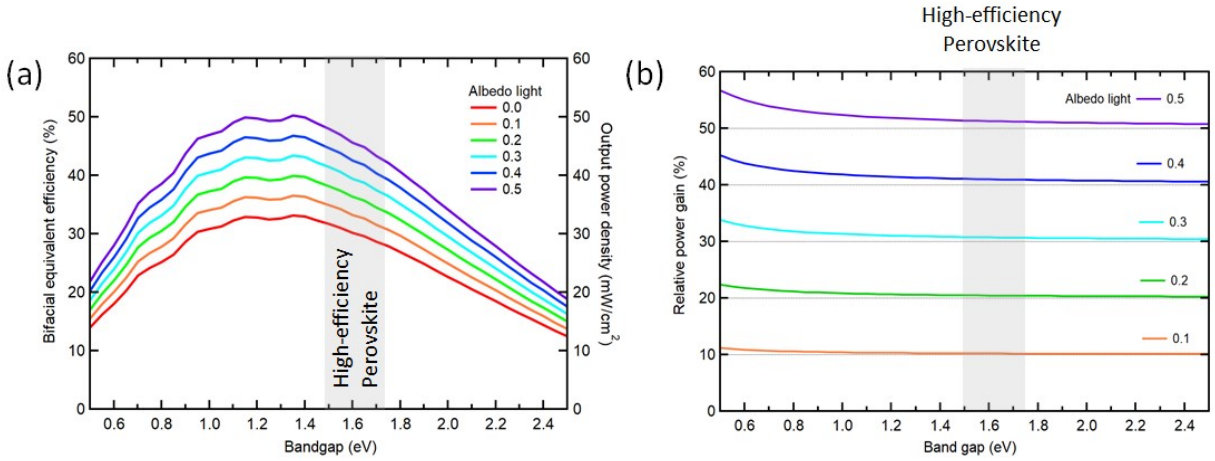

Figure S6. (a) Detailed balance bifacial equivalent efficiency (output power density) and (b) relative power gains of bifacial solar cells with different bandgaps under various albedo light conditions. The shaded area highlights the bandgap range for high-efficiency perovskite solar cells. Note that an albedo of 0.5 is close to a white fiberglass rooftop surface. The condition of snow is not considered because of the limited time and location for snow-covered surfaces.

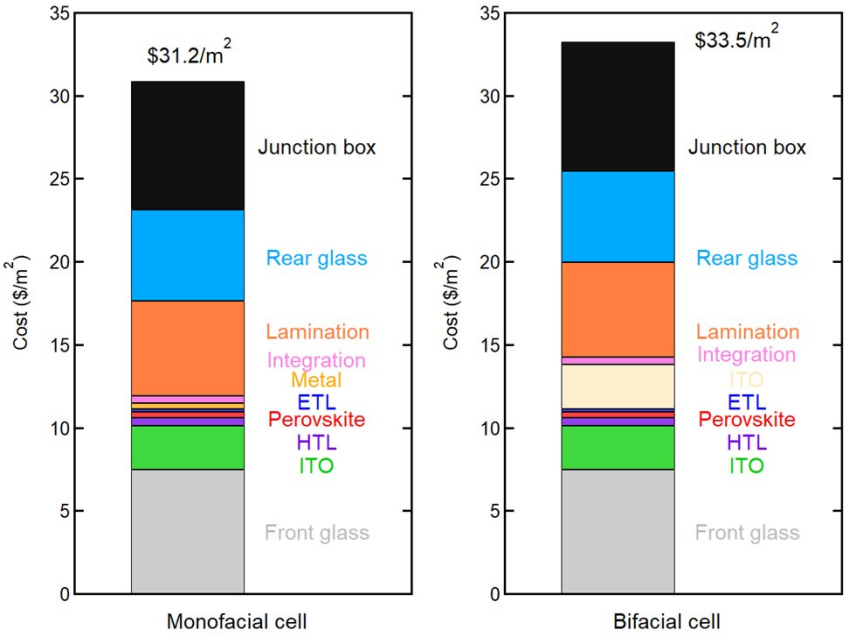

Figure S7. Manufacturing costs estimation of monofacial and bifacial PSCs. The cost data is adapted from our previous report.[16]

References

1. C. Chen, Z. Song, C. Xiao, R. A. Awni, C. Yao, N. Shrestha, C. Li, S. S. Bista, Y. Zhang, L. Chen, R. J. Ellingson, C.-S. Jiang, M. Al-Jassim, G. Fang and Y. Yan, *ACS Energy Lett.*, 2020, **5**, 2560-2568.
2. Z. Yu, Z. Yang, Z. Ni, Y. Shao, B. Chen, Y. Lin, H. Wei, Z. J. Yu, Z. Holman and J. Huang, *Nat. Energy*, 2020, **5**, 657-665.
3. W. Shockley and H. J. Queisser, *Journal of Applied Physics*, 1961, **32**, 510-519.
4. A. M. Baldridge, S. J. Hook, C. I. Grove and G. Rivera, *Remote Sensing of Environment*, 2009, **113**, 711-715.
5. M. A. Green, *Solid-State Electronics*, 1981, **24**, 788-789.
6. T. Li, W. A. Dunlap-Shohl and D. B. Mitzi, *ACS Appl. Energy Mater.*, 2020, **3**, 9493-9497.
7. F. Liang, Z. Ying, Y. Lin, B. Tu, Z. Zhang, Y. Zhu, H. Pan, H. Li, L. Luo, O. Ageev and Z. He, *Adv. Mater. Interfaces*, 2020, **7**, 2000591.
8. H. Wang, H. A. Dewi, T. M. Koh, A. Bruno, S. Mhaisalkar and N. Mathews, *ACS Appl. Energy Mater.*, 2020, **12**, 484-493.
9. D. Chen, S. Pang, L. Zhou, X. Li, A. Su, W. Zhu, J. Chang, J. Zhang, C. Zhang and Y. Hao, *J. Mater. Chem. A*, 2019, **7**, 15156-15163.
10. Y. Cheng, C. Xie, X. Liu, G. Zhu, H.-W. Li, S. Venkataraj, Z.-K. Tan, L. Ding, A. G. Aberle and F. Lin, *Science Bulletin*, 2020, **65**, 607-610.
11. A. J. Bett, K. M. Winkler, M. Bivour, L. Cojocaru, Ö. Ş. Kabakli, P. S. C. Schulze, G. Siefer, L. Tutsch, M. Hermle, S. W. Glunz and J. C. Goldschmidt, *ACS Appl. Energy Mater.*, 2019, **11**, 45796-45804.
12. S. Pang, X. Li, H. Dong, D. Chen, W. Zhu, J. Chang, Z. Lin, H. Xi, J. Zhang, C. Zhang and Y. Hao, *ACS Appl. Energy Mater.*, 2018, **10**, 12731-12739.
13. C. Hanmandlu, C.-Y. Chen, K. M. Boopathi, H.-W. Lin, C.-S. Lai and C.-W. Chu, *ACS Appl. Energy Mater.*, 2017, **9**, 32635-32642.

14. Y. Li, J. Duan, Y. Zhao and Q. Tang, *Chem. Commun.*, 2018, **54**, 8237-8240.
15. F. Fu, T. Feurer, T. P. Weiss, S. Pisoni, E. Avancini, C. Andres, S. Buecheler and A. N. Tiwari, *Nat. Energy*, 2016, **2**, 16190.
16. Z. Song, C. L. McElvany, A. B. Phillips, I. Celik, P. W. Krantz, S. C. Watthage, G. K. Liyanage, D. Apul and M. J. Heben, *Energy Environ. Sci.*, 2017, **10**, 1297-1305.